NULL | null | JCA11.2.5208/W Library-x64 | manuscript.3f (R5.0.i3:5004 | 2.1) 2020/02/05 13:43:00 | PROD-WS-120 | rq_3184314 | 8/31/2020 13:38:06 | 7 | JCA-DEFAULT

ACS Macro Letters

pubs.acs.org/macroletters Letter

Core–Shell Microfibers via Bioorthogonal Layer-by-Layer Assembly

Anitha Ravikrishnan,[∥] He Zhang,[∥] Joseph M. Fox,* and Xinqiao Jia*

Cite This: https://dx.doi.org/10.1021/acsmacrolett.0c00515 Read Online

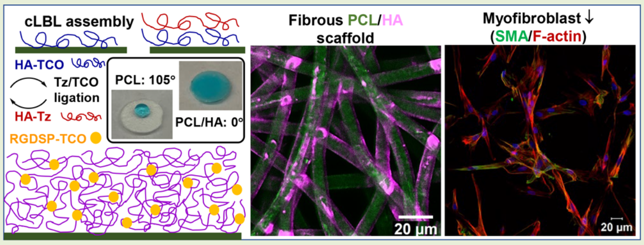

ABSTRACT: A new technique is described for the construction of core–shell microfibers for biomedical applications. Fibrous scaffolds were fabricated by electrospinning, followed by covalent layer-by-layer deposition based on the rapid bioorthogonal reaction between *s*-tetrazines (Tz) and *trans*-cyclooctenes (TCOs). Electrospun poly(ε-caprolactone) (PCL) scaffolds were subjected to surface modifications to install tetrazine groups. The scaffolds were iteratively submerged in aqueous solutions of TCO-modified hyaluronic acid (HA-TCO) and tetrazine-modified hyaluronic acid (HA-Tz), resulting in the controlled growth of a cross-linked HA gel around individual microfibers. Integrin-binding motifs were covalently attached to the surface of the microfibers using TCO-conjugated RGD peptide. The scaffolds fostered the attachment and growth of primary porcine vocal fold fibroblasts without a significant induction of the myofibroblast phenotype. Stimulation with transforming growth factor beta (TGF-β) moderately enhanced fibroblast activation, and inhibition of the Rho/ROCK signaling pathway using Y27632 further decreased the expression of myofibroblastic markers. The bioorthogonally assembled scaffolds with a stiff PCL core and a soft HA shell may find application as therapeutic implants for the treatment of vocal fold scarring.

The vocal fold consists of a soft connective tissue (lamina propria), sandwiched between a stratified squamous epithelium and the vocalis muscle.[1] Sound is produced when vocal folds oscillate regularly in a wave-like motion at frequencies of 100–1000 Hz. Vocal folds can be damaged by chemical, pathological, and mechanical insults. In response to injury, fibroblasts migrate to the wound bed and become activated to myofibroblasts, which synthesize excessive extracellular matrix (ECM) proteins, develop α-smooth muscle actin (αSMA), and exert traction forces on the ECM. At the end of the remodeling process when the wound closes, myofibroblasts disappear by apoptosis. However, in pathological situations, myofibroblasts persist, proliferate, and develop excessive tissue contraction, leading to chronic fibrosis or hypertrophic scarring that is challenging to treat.[2,3]

Synthetic scaffolds, if appropriately designed, can be used to promote constructive tissue remodeling and repair.[4] In this context, therapeutic scaffolds can be introduced to the lamina propria via minimally invasive microflap surgery to actively mediate the fibrotic responses, ultimately regenerating the normal tissue composition, microstructure, and viscoelasticity.[5] Electrospun fibrous scaffolds mimic the architecture of the natural ECM and present biochemical and topographical cues that modulate cell differentiation during wound healing.[6] Fibrous scaffolds of varying fiber diameter have been produced using poly(ε-caprolactone) (PCL).[7] Although mechanically robust, these scaffolds are bioinert and are several orders of magnitude stiffer than the vocal fold.[8] Injection of PCL-based microspheres in the muscle have been proposed for the treatment of glottal insufficiency.[9] However, little is known about the fibrogenic and inflammatory responses of resident vocal fold fibroblasts (VFFs) to pristine PCL scaffolds implanted superficially in the lamina propria.

On the other hand, hyaluronic acid (HA) is naturally enriched in the vocal fold lamina propria, contributing to the maintenance of optimal tissue viscoelasticity, regulating cell functions through binding with cell surface HA receptors, and promoting scarless wound healing in fetal tissues.[10,11] However, electrospinning of HA is challenging because it is highly charged and has limited solubility in volatile organic solvents.[12] Even with its high molecular weight, a carrier polymer, such as poly(ethylene oxide), is often required to produce continuous fibers.[13] Covalent cross-linking is necessary to maintain mechanical resistance and structural integrity when hydrated.[14]

Here, we describe the synthesis of fibrous PCL/HA scaffolds with a core–shell configuration. Our design takes advantage of the semicrystalline nature of PCL to maintain structural and mechanical integrity of the scaffold.[15] Individual PCL fibers were encased in a soft HA shell to foster cell–ECM interactions and to modulate cell phenotypes. Fibrous PCL/chitosan scaffolds have been produced by electrospinning and layer-by-layer (LBL) deposition.[16] Conventional LBL assembly

Received: July 13, 2020
Accepted: August 28, 2020

involves alternate deposition of complementary charged polymeric species via electrostatic interactions.[17] Because the resultant multilayered films were held together by weak noncovalent interactions, long-term *in vivo* stability of the coating is not guaranteed. To improve stability, covalent LBL (cLBL) assembly has been developed. In this case, the building blocks do not have to be oppositely charged, and spatiotemporal conjugation of bioactive compounds of low and high molecular weight is possible.[18]

Bioorthogonal reactions, such as Staudinger ligation, copper(I)-catalyzed azide−alkyne cycloadditions, and strain-promoted azide−alkyne cycloadditions, have been explored for surface modification and cell encapsulation in a LBL fashion.[19] To ensure rapid growth of the HA gel layer, the reaction should occur instantaneously under mild conditions. Tetrazine ligation, the inverse electron demand Diels−Alder cycloaddition reaction between a strained *trans*-cyclooctene (TCO) and *s*-tetrazine (Tz), is biocompatible, high yielding, and extremely fast (second-order rate constant, k_2, exceeding 10^4 M^{-1} s^{-1}) and does not require any catalyst, nor does it exhibit cross reactivity with endogenous biomacromolecules.[20−22] We have successfully applied this chemistry to the creation of protein-mimetic polymeric microfibers[23−25] and 3D biomimetic environments with well-defined spatiotemporal signals.[26−29]

Herein, we took advantage of the exceptional kinetics of tetrazine ligation to produce fibrous scaffolds with a stiff PCL core and a soft HA shell via cLBL assembly. PCL scaffolds with an average fiber diameter of 3.80 ± 0.27 μm (Figure S1), comparable to that of the collagen fibers (4 μm) present during the remodeling phase of the wound healing process,[30] were consistently produced following our standard electrospinning protocol.[7,31] Individual fibers were randomly oriented and intimately entangled, creating microsized interstitial pores. Fiber surfaces were relatively smooth and free of any nanoscale topography. Separately, HA derivatives with bioorthogonal handles were synthesized following our reported procedures (Scheme S1 and Figure 1A).[27−29] By ^{1}H NMR, HA-Tz had a 23% tetrazine incorporation, and HA-TCO had a degree of modification of 25% (Figure S2). To introduce integrin-binding sites on the fibrous scaffold, the monofunctional TCO conjugate, RGD−TCO, was synthesized following our reported solid-phase synthesis protocol (Figures S3 and S4).[24,27] To ensure robust attachment of HA to PCL, scaffolds were subjected to surface modification to install Tz functionality (PCL-Tz) prior to cLBL deposition (Figure 1A). A 30 min incubation of PCL-Tz in the HA-TCO bath led to the deposition of the first HA layer (PCL/HA1). The scaffold was then immersed in the HA-Tz bath for 5 min to afford PCL/HA2. The process was repeated up to 60 times, with a 5 min immersion in each bath, to establish a covalently cross-linked HA shell around individual PCL fibers (PCL/HA, *n*, *n* = 1−60). After the final dipping in the HA-Tz bath, the scaffolds were washed with PBS three times and transferred to an RGD-TCO bath to introduce recognition sequences for integrins (Figure 1B).

UV−vis analysis was conducted on the HA-Tz bath during the cLBL process to confirm the immobilization of HA on the PCL microfibers. HA-Tz concentration was determined based on the absorbance at 265 nm by Beer−Lambert law, taking into consideration the molar extinction coefficient of the Tz-hydrazide as 23,500 M^{-1}.[27] Figure 2A shows the UV−vis absorbance spectra of the HA-Tz bath after 0 to 60 times of

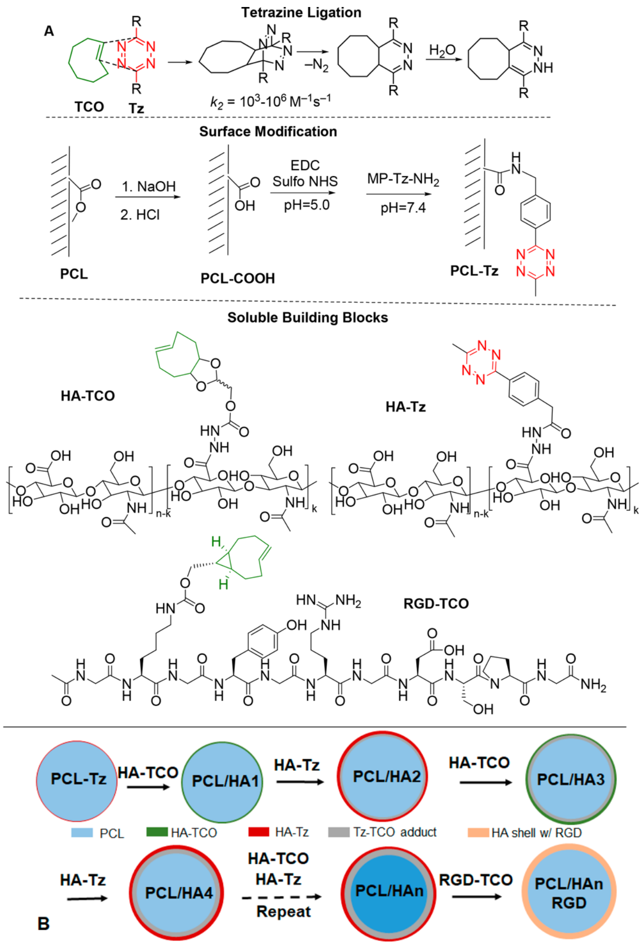

Figure 1. (A) Tetrazine ligation with TCO features bioorthogonality and unprecedented rate. Prior to cLBL assembly, the electrospun PCL scaffold was subjected to surface modification to install the tetrazine group. Hydrogel building blocks include HA-Tz, HA-TCO, and RGD-TCO. (B) Schematic depiction of the cLBL process, shown in a cross-sectional view. *n*: number of times the scaffold was exposed to HA baths.

exposure. There is a progressive decrease in absorbance as *n* increases. This corresponds to a decrease of HA-Tz concentration from 1.3 mM before the cLBL process was initiated, to 0.5 mM when the process was terminated. This result shows that during the cLBL process HA-Tz was progressively depleted from the bath and deposited on the scaffold.

The surface modification and HA conjugation were further evaluated by XPS (Figure 2B). Only C_{1s} and O_{1s} signals were detected on virgin PCL scaffolds, consistent with the chemical composition of PCL. After the tetrazine group was introduced, a nitrogen peak was detected at 400 eV. A sodium peak (1071 eV) appeared when *n* = 2, and its intensity did not alter significantly as the cLBL process progressed. The appearance of Na_{1s} confirms the immobilization of HA on the scaffold because HA used in this study was in the form of sodium salt. XPS is a surface-sensitive technique. With a 90° takeoff angle, the sampling depth ranges from 6 to 12 nm.[32] Therefore, as *n* increased from 2 to 60, XPS did not reveal any additional changes in surface chemical composition. The fibrous nature of the scaffolds prohibits depth-dependent quantitative interpretation of the XPS results.

https://dx.doi.org/10.1021/acsmacrolett.0c00515
ACS Macro Lett. XXXX, XXX, XXX−XXX

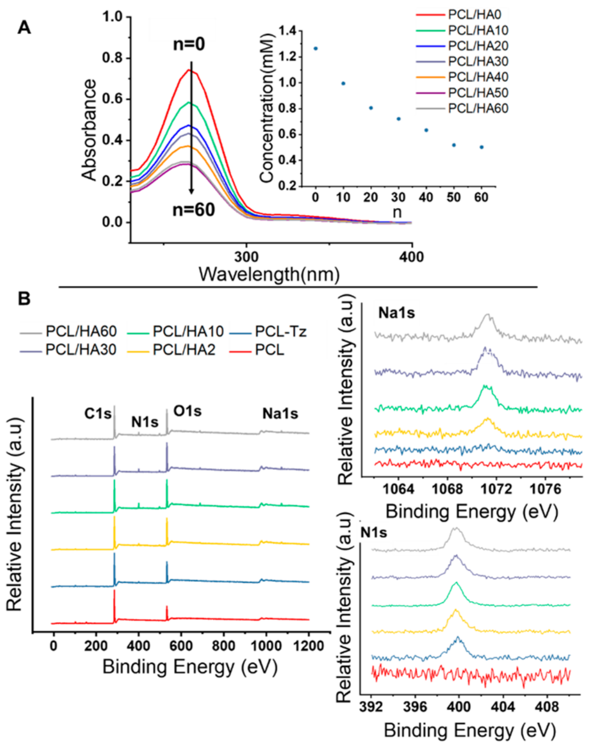

Figure 2. Characterization of fibrous PCL/HA scaffolds by UV−vis (A) and XPS (B). (A) UV−vis absorption spectra of the HA-Tz bath used for the assembly of the HA gel. As *n* increased, the absorbance at 265 nm decreased, indicating removal of the tetrazine species from the bath. The inset shows HA-Tz concentration as a function of *n*. (B) XPS survey (left) and high-resolution (right) Na_{1s} and N_{1s} spectra of PCL/HA. Compared to pristine PCL, PCL/HA exhibited characteristic nitrogen (from tetrazine) and sodium (from HA) peaks.

Change in surface hydrophobicity was analyzed by contact angle measurement using a sessile drop method (Figure 3A). Without any chemical modifications, PCL scaffolds were hydrophobic, having a contact angle of 104.9 ± 5.5°. After being exposed to HA baths 60 times, the scaffold (PCL/HA60) exhibited a zero-degree contact angle, indicating a significant improvement in hydrophilicity. Thus, the cLBL process established a cohesive hydrogel layer on the PCL fibers. Visually, water beaded up on virgin PCL scaffolds, unable to penetrate into the scaffold (inset, PCL, Figure 3A). With the addition of HA coating, water rapidly spread out and became adsorbed by the scaffold. As the cLBL process continued, the scaffold gradually became translucent (inset, PCL/HA60, Figure 3A), adopted a gel-like appearance, and became slippery. Unlike PCL/HA60, water distribution on PCL/HA2 was patchy and uneven (inset, PCL/HA2, Figure 3A), suggesting inhomogeneous or incomplete surface coverage by HA.

SEM characterization (Figure 3B) confirmed that the cLBL process did not affect fiber morphology; fibers remained uniform and smooth. PCL, PCL/HA2, and PCL/HA60 exhibited similar mechanical properties, as assessed by tensile tests using a dynamic mechanical analyzer (DMA). Young's modulus, calculated based on the linear portion of the stress−strain curves measured by DMA (Figure S5), was 9.49 ± 0.76, 9.44 ± 0.86, and 9.09 ± 0.72 MPa for PCL, PCL/HA2, and PCL/HA60, respectively. These values are statistically indistinguishable. Therefore, the surface modification did not alter the stiffness of the scaffolds. In this context, the tensile

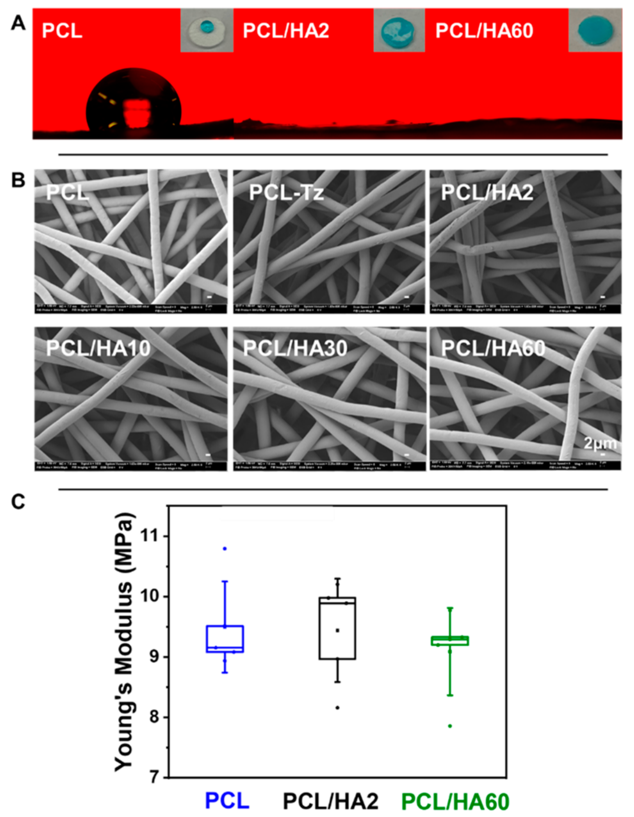

Figure 3. Characterization of fibrous PCL/HA scaffolds by contact angle goniometry (A), SEM (B), and DMA (C). (A) Change in the surface hydrophilicity was monitored by the sessile drop method. Insets show the appearance of the scaffolds 5 min after the addition of water with blue food dye. (B) SEM analysis confirmed that scaffold morphology was not affected by surface modifications. (C) Scaffolds with *n* = 0, 2, and 60 exhibited similar Young's modulus, suggesting that surface modification did not affect the bulk property of the scaffolds.

modulus of a solvent-cast PCL specimen is 123 MPa,[33] whereas the Young's modulus of an HA gel prepared via interfacial cross-linking using Tz/TCO ligation is 16 kPa.[27]

To confirm the core−shell architecture, the HA shell was stained green using biotinylated hyaluronan binding protein (HABP-Biotin) and Alexa Fluor 488-conjugated streptavidin (Alexa-Strep), and the PCL core was stained red by CellTracker Red.[7] The presence of a cohesive HA sheath around the PCL core is evident (Figure 4A). No Alexa signal was detected from as-spun PCL scaffolds without any treatment. Although an accurate determination of the thickness of the HA shell based on the confocal image was not possible, a rough estimate suggested the presence of a submicron gel coating around the PCL core after the scaffold was exposed to HA baths 60 times. In the last step of the cLBL process, scaffolds were immersed in an RGD-TCO solution for 1 h to immobilize the cell-adhesive ligands. To model the peptide conjugation, Cy5-TCO was used in place of RGD-TCO to provide a fluorescent signal for confocal imaging. Cy5-TCO and RGD-TCO have comparable molecular weight, diffusivity, and aqueous solubility.[29] To provide contrast, the PCL core was stained with Hoechst[34,35] and false colored as green in Figure 4B for easy visualization. Our results show diffuse Cy5 signals around the PCL fibers. We reason that, during the 1 h incubation, Cy5-TCO readily diffuses into the HA layer,

https://dx.doi.org/10.1021/acsmacrolett.0c00515
ACS Macro Lett. XXXX, XXX, XXX−XXX

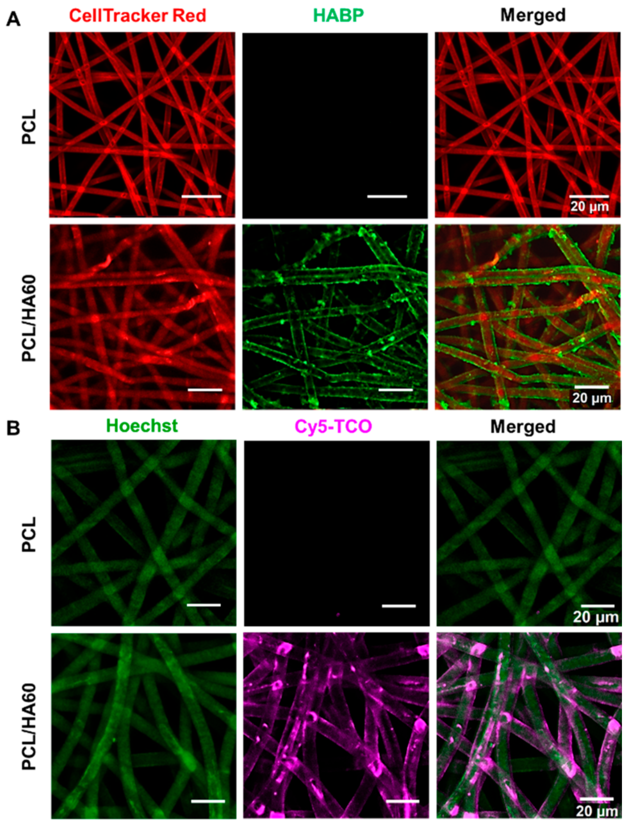

Figure 4. Characterization of the fibrous PCL/HA60 scaffold by confocal microscopy. (A) The core–shell structure was confirmed by staining the HA shell with HABP-biotin/Alexa-Strep (green) and the PCL core with CellTracker Red (red). (B) Cy5-TCO (pink) was used as a surrogate for RGD-TCO to confirm peptide conjugation. The PCL core was stained by Hoechst and false colored as green for easy visualization.

reacting with residual tetrazine groups through tetrazine ligation. Again, no Cy5 signal was detected for unmodified PCL scaffolds.

Collectively, bioorthogonal deposition of HA on PCL microfibers resulted in the formation of a cell-adhesive scaffold with a core–shell structure. The cLBL process profoundly altered the surface composition without changing the fiber morphology or matrix stiffness. Cell-adhesive peptide was conjugated throughout the gel layer. Because Tz/TCO reaction is quantitative and instantaneous,[36] the buildup of the HA shell is fast; washing and liquid transfer is the rate-limiting step, which can be sped up using an automated liquid handling system. Considering the robustness and homogeneity of the HA coating, PCL/HA60 was used in subsequent cell culture studies. PCL/HA2 was included as a negative control.

To assess the therapeutic efficacy of the scaffolds, culture-expanded VFFs were cultured on the scaffolds under various conditions for a total of 7 days (Table S1). One day after plating, cells were subjected to 3-day culture with or without TGF-β, a potent pro-fibrotic cytokine. TGF-β plays an important role in inducing differentiation of fibroblasts to myofibroblasts by increasing contractile forces generated from the actin stress fibers.[37] Subsequently, cells were cultured for 3 days with or without Y27632, a potent, selective inhibitor of ROCK and myosin type II contractility, thereby inhibiting myofibroblastic differentiation.[38]

Primary VFFs were isolated from porcine vocal folds and expanded on conventional tissue culture polystyrene (TCPS). Under these conditions, VFFs acquired the myofibroblast phenotype, as evidenced by the colocalization of αSMA signals with mature F-actin stress fibers (Figure S6A). Increased expression of αSMA correlates with increased generation of contractile forces.

By ImageJ, 95.6 ± 1.2% of cells were αSMA+. In agreement with prior reports, exposing cells to a nonphysiologically stiff plastic substrate (~2 GPa) triggered the formation of contractile stress fibers,[39,40] thereby promoting myofibroblast differentiation. As expected, Y27632 overrode the substrate effects, inhibiting the development of stress fibers and the expression of αSMA (Figure S6B). These TCPS-primed, αSMA+ cells are phenotypically similar to scarred VFFs[41] and thus are physiologically relevant.

VFFs cultured on PCL/HA60 scaffolds maintained high viability (87–95%) throughout the 7-day period, as evidenced by live/dead staining (Figure 5A). By day 7, viable cells

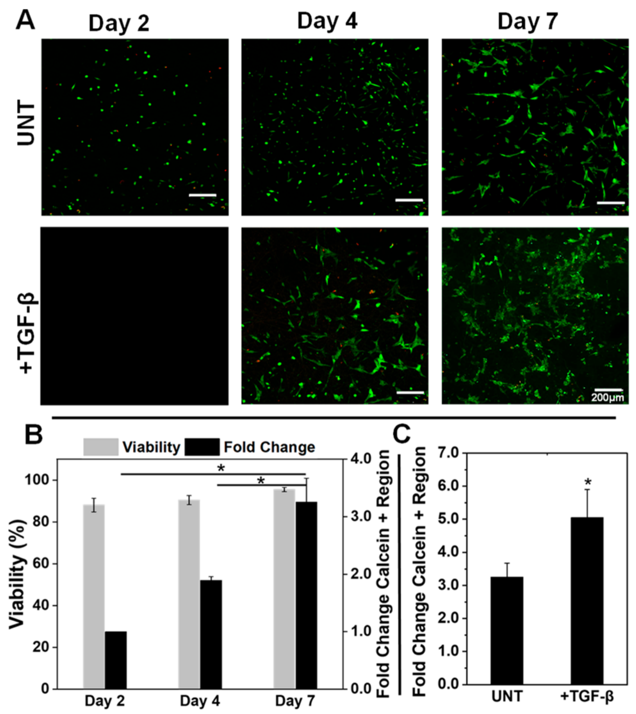

Figure 5. Characterization of VFFs cultured on fibrous PCL/HA60 scaffolds by live/dead staining. (A) Representative confocal images showing live cells stained green by calcein AM and dead cells stained red by ethidium homodimer, respectively, after 2, 4, and 7 days of culture. (B) Quantification of viability and proliferation as a function of culture time. (C) Effect of TGF-β treatment on cell proliferation on day 7. Percent viability was quantified based on the confocal images using ImageJ. Cell proliferation is expressed as fold change in calcein positive regions normalized to day 2. Quantification was carried out using ImageJ software based on three separate 1024 × 1024 μm^2 confocal images. *: Significantly different ($p < 0.05$, ANOVA). Error represents standard error of the mean of three repeats.

consitituted 95.5 ± 1.1% of the cell population (Figure 5B). Robust cell proliferation was observed on the scaffolds, with a 2- and 4-fold increase in cell number by day 4 and day 7, respectively (Figure 5B). Supplementation of the culture on day 2 with TGF-β led to a 1.5-fold increase in cell proliferation (Figure 5C). Y27632 at 1000 nM did not affect the viability of

https://dx.doi.org/10.1021/acsmacrolett.0c00515
ACS Macro Lett. XXXX, XXX, XXX−XXX

VFFs (Figure S7), in agreement with previous reports.[38,42] Cells maintained on PCL/HA2 exhibited a similar pattern of viability and growth (Figure S8).

Next, we evaluated cell phenotype by immunostaining for αSMA, a myofibroblastic marker (Figure 6A, Figure S10A). By day 7, only 27.5 ± 0.6% cells seeded on PCL/HA60 scaffolds expressed αSMA (UNT). Upon stimulation with TGF-β, the percentage of αSMA+ cells on PCL/HA60 increased to 63.1 ± 0.8% (+TGF-β). Cells cultured with Y27632 showed weak and diffuse αSMA/F-actin staining. On average, 10.6 ± 0.4% cells were αSMA+ (+ROCKi). Introduction of Y27632 after a 3-day TGF-β stimulation significantly suppressed the myofibroblast differentiation; the inductive effect of TGF-β was attenuated. On average, 26.4 ± 0.7% of cells were αSMA+ (+TGF-β/+ROCKi). By contrast, a higher perecentage of cells cultured on HA/PCL2 were αSMA+ under all conditions (Figures S9A and S10B).

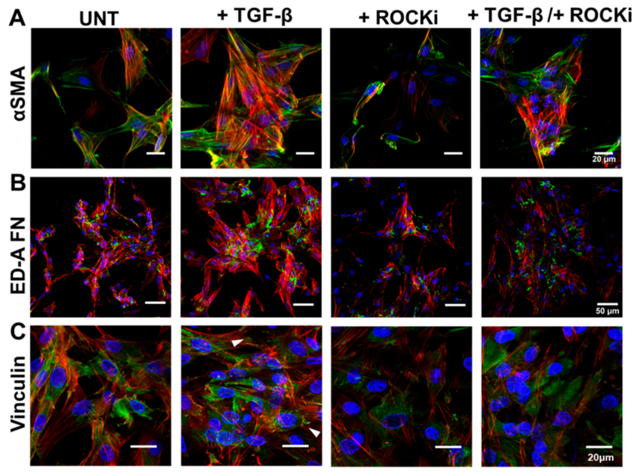

Figure 6. Representative confocal images of day 7 cultures on PCL/HA60, showing nuclei and F-actin stained blue and red, respectively. αSMA (A), ED-A FN (B), and vinculin (C) were stained green. White arrowheads indicate the point at which vinculin overlaps with the F-actin fibers at the tip of the filopodia.

The production of ED-A FN indicates the onset of myofibroblast differentiation.[3] In the absence of TGF-β or Y27632, cells secreted very little ED-A FN (Figure 6B). TGF-β stimulation resulted in a 3.5-fold increase in the upregulation of ED-A FN (Figure S11A) and induced the bundling of ED-A FN fibers.[43] Exposure of cells to Y27632, but not to TGF-β, reduced the synthesis of ED-A FN by 57.5 ± 1.1%. When we primed the VFFs with TGF-β, Y27632 reduced ED-A FN production by 44.7 ± 1.0%. On the other hand, cells on PCL/HA2 consistently expressed a higher level of the protein even in the presence of Y27632 (Figures S9B amd 11B).

During myofibroblast differentiation, the expression of αSMA is associated with formation of large mature focal adhesions (FAs).[44] Vinculin is a major cytoplasmic FA protein that regulates the cell migration and traction forces during wound healing.[45] Vinculin staining on cells on PCL/HA60 was intracellular and diffuse (Figure 6C). Even when treated with TGF-β, we only observed a few isolated regions with localization of vinculin to the periphery of the cells as puncta. Inhibition with Y27632 led to the disassembly of F-actin stress fibers, thereby decreasing focal adhesion sites on the scaffolds. When primed with the soluble growth factor, ROCK inhibition resulted in the cytoplasmic translocation of vinculin. It has been shown that TGF-β increased the expression of integrin receptors and vinculin-containing focal adhesion complexes with the recruitment of stress fibers. By comparison, cells cultured on PCL/HA2 developed distinct and mature FA complexes, with vinculin localized at the extremities of the F-actin stress fibers in a discrete punctuated pattern (Figure S9C). Our results confirm the ability of fibrous PCL/HA60 scaffolds to suppress/reverse myofibroblast differentiation and highlight the need for complete encasement of the PCL fiber with a thick, coheasive HA shell.

In summary, microfibrous scaffolds with a stiff PCL core and a soft HA shell were fabricated by electrospinning and tetrazine ligation-mediated cLBL assembly. The fast tetrazine ligation enabled rapid and robust growth of the HA shell without any catalyst or external triggers. The resultant scaffolds supported the attachment and growth of TCPS-primed VFFs and effectively suppressed myofibroblast differentiation. Our results suggest that priming scar tissues with a fibrous patch that is mechanically robust but contains a soft and compliant HA coating will effectively suppress the fibrogenesis and promote tissue repair. To further enhance the therapeutic efficacy, antifibrotic drugs, such as pirfenidone and hepatocyte growth factor, can be loaded in the PCL core and HA shell for sustained release. Overall, the scaffold is designed to modulate the ECM environment and cellular programs to antagonize myofibroblast differentiation and promote the growth of healthy tissues.

■ ASSOCIATED CONTENT

Supporting Information

The Supporting Information is available free of charge at https://pubs.acs.org/doi/10.1021/acsmacrolett.0c00515.

A list of abbreviations, experimental procedures, SEM characterization of the pristine PCL scaffold, ^{1}H NMR and mass spectrometry characterization of HA-Tz, HA-TCO, and RGD-TCO, stress−strain curves of various scaffolds, confocal images of VFFs cultured on TCPS or PCL/HA scaffolds, and quantitation of αSMA and ED-A FN expression (PDF)

■ AUTHOR INFORMATION

Corresponding Authors

Xinqiao Jia − *Departments of Materials Science and Engineering, University of Delaware, Newark, Delaware 19716, United States;* orcid.org/0000-0002-3564-5576; Email: xjia@udel.edu

Joseph M. Fox − *Department of Chemistry and Biochemistry, University of Delaware, Newark, Delaware 19716, United States;* orcid.org/0000-0002-8258-1640; Email: jmfox@udel.edu

Authors

Anitha Ravikrishnan − *Departments of Materials Science and Engineering, University of Delaware, Newark, Delaware 19716, United States;* orcid.org/0000-0002-2385-563X

He Zhang − *Departments of Materials Science and Engineering, University of Delaware, Newark, Delaware 19716, United States*

Complete contact information is available at: https://pubs.acs.org/10.1021/acsmacrolett.0c00515

https://dx.doi.org/10.1021/acsmacrolett.0c00515
ACS Macro Lett. XXXX, XXX, XXX−XXX

Author Contributions

‖A.R. and H.Z. contributed equally.

Notes

The authors declare no competing financial interest.

■ ACKNOWLEDGMENTS

This work was supported in part by the National Institutes of Health (NIDCD, R01DC014461), National Science Foundation (NSF, DMR 1809612), and Delaware Bioscience Center. Instrumentation was supported by NIH grants P30GM110758, P20GM104316, S10RR026962, and S10OD016267 and NSF grants CHE-0840401, CHE-1229234, and CHE-1048367. We acknowledge Sanofi-Genzyme for generously providing HA. We thank Dr. Jeffrey Caplan for his assistance with confocal imaging, Mr. Wenbo Wu for his advice on XPS analysis, Dr. Yong Zhao for his guidance in SEM characterization, and Dr. Robert Mauck for providing porcine larynxes.

■ REFERENCES

(1) Gray, S. D. Cellular Physiology of the Vocal Folds. *Otolaryngol. Clin. North Am.* **2000**, *33*, 679−698.

(2) Friedrich, G.; Dikkers, F. G.; Arens, C.; Remacle, M.; Hess, M.; Giovanni, A.; Duflo, S.; Hantzakos, A.; Bachy, V.; Gugatschka, M. Vocal Fold Scars: Current Concepts and Future Directions. Consensus Report of the Phonosurgery Committee of the European Laryngological Society. *Eur. Arch Otorhinolaryngol* **2013**, *270*, 2491−2507.

(3) Darby, I. A.; Laverdet, B.; Bonté, F.; Desmoulière, A. Fibroblasts and Myofibroblasts in Wound Healing. *Clin., Cosmet. Invest. Dermatol.* **2014**, *7*, 301−311.

(4) Li, L.; Stiadle, J. M.; Lau, H. K.; Zerdoum, A. B.; Jia, X.; Thibeault, S. L.; Kiick, K. L. Tissue Engineering-Based Therapeutic Strategies for Vocal Fold Repair and Regeneration. *Biomaterials* **2016**, *108*, 91−110.

(5) Kishimoto, Y.; Welham, N. V.; Hirano, S. Implantation of Atelocollagen Sheet for Vocal Fold Scar. *Curr. Opin. Otolaryngol Head Neck Surg.* **2010**, *18*, 507−511.

(6) Rieger, K. A.; Birch, N. P.; Schiffman, J. D. Designing Electrospun Nanofiber Mats to Promote Wound Healing−A Review. *J. Mater. Chem. B* **2013**, *1*, 4531−4541.

(7) Ravikrishnan, A.; Ozdemir, T.; Bah, M.; Baskerville, K. A.; Shah, S. I.; Rajasekaran, A. K.; Jia, X. Regulation of Epithelial-to-Mesenchymal Transition Using Biomimetic Fibrous Scaffolds. *ACS Appl. Mater. Interfaces* **2016**, *8*, 17915−17926.

(8) Jiang, L.; Jiang, Y.; Stiadle, J.; Wang, X.; Wang, L.; Li, Q.; Shen, C.; Thibeault, S. L.; Turng, L. S. Electrospun Nanofibrous Thermoplastic Polyurethane/Poly(Glycerol Sebacate) Hybrid Scaffolds for Vocal Fold Tissue Engineering Applications. *Mater. Sci. Eng., C* **2019**, *94*, 740−749.

(9) Kwon, S. K.; Kim, H. B.; Song, J. J.; Cho, C. G.; Park, S. W.; Choi, J. S.; Ryu, J.; Oh, S. H.; Lee, J. H. Vocal Fold Augmentation with Injectable Polycaprolactone Microspheres/Pluronic F127 Hydrogel: Long-Term in Vivo Study for the Treatment of Glottal Insufficiency. *PLoS One* **2014**, *9*, No. e85512.

(10) Chan, R. W.; Gray, S. D.; Titze, I. R. The Importance of Hyaluronic Acid in Vocal Fold Biomechanics. *Otolaryngol.–Head Neck Surg.* **2001**, *124*, 607−614.

(11) Dicker, K. T.; Gurski, L. A.; Pradhan-Bhatt, S.; Witt, R. L.; Farach-Carson, M. C.; Jia, X. Hyaluronan: A Simple Polysaccharide with Diverse Biological Functions. *Acta Biomater.* **2014**, *10*, 1558−1570.

(12) Lee, K. Y.; Jeong, L.; Kang, Y. O.; Lee, S. J.; Park, W. H. Electrospinning of Polysaccharides for Regenerative Medicine. *Adv. Drug Delivery Rev.* **2009**, *61*, 1020−1032.

(13) Kim, I. L.; Khetan, S.; Baker, B. M.; Chen, C. S.; Burdick, J. A. Fibrous Hyaluronic Acid Hydrogels That Direct Msc Chondrogenesis through Mechanical and Adhesive Cues. *Biomaterials* **2013**, *34*, 5571−5580.

(14) Collins, M. N.; Birkinshaw, C. Hyaluronic Acid Based Scaffolds for Tissue Engineering - A Review. *Carbohydr. Polym.* **2013**, *92*, 1262−1279.

(15) Iroh, J. O. Poly(Epslon-Caprolactone). In *Polymer Data Handbook*; Mark, J. E., Ed.; Oxford University Press: New York, 1999; pp 361−362.

(16) Croisier, F.; Sibret, P.; Dupont-Gillain, C. C.; Genet, M. J.; Detrembleur, C.; Jérôme, C. Chitosan-Coated Electrospun Nanofibers with Antibacterial Activity. *J. Mater. Chem. B* **2015**, *3*, 3508−3517.

(17) Hammond, P. T. Form and Function in Multilayer Assembly: New Applications at the Nanoscale. *Adv. Mater.* **2004**, *16*, 1271−1293.

(18) An, Q.; Huang, T.; Shi, F. Covalent Layer-by-Layer Films: Chemistry, Design, and Multidisciplinary Applications. *Chem. Soc. Rev.* **2018**, *47*, 5061−5098.

(19) Gattas-Asfura, K. M.; Stabler, C. L. Bioorthogonal Layer-by-Layer Encapsulation of Pancreatic Islets Via Hyperbranched Polymers. *ACS Appl. Mater. Interfaces* **2013**, *5*, 9964−9974.

(20) Blackman, M. L.; Royzen, M.; Fox, J. M. Tetrazine Ligation: Fast Bioconjugation Based on Inverse-Electron-Demand Diels− Alder Reactivity. *J. Am. Chem. Soc.* **2008**, *130*, 13518−13519.

(21) Devaraj, N. K.; Weissleder, R.; Hilderbrand, S. A. Tetrazine-Based Cycloadditions: Application to Pretargeted Live Cell Imaging. *Bioconjugate Chem.* **2008**, *19*, 2297−2299.

(22) Darko, A.; Wallace, S.; Dmitrenko, O.; Machovina, M. M.; Mehl, R. A.; Chin, J. W.; Fox, J. M. Conformationally Strained Trans-Cyclooctene with Improved Stability and Excellent Reactivity in Tetrazine Ligation. *Chem. Sci.* **2014**, *5*, 3770−3776.

(23) Liu, S.; Zhang, H.; Remy, R. A.; Deng, F.; Mackay, M. E.; Fox, J. M.; Jia, X. Meter-Long Multiblock Copolymer Microfibers Via Interfacial Bioorthogonal Polymerization. *Adv. Mater.* **2015**, *27*, 2783−2790.

(24) Zhang, H.; Trout, W. S.; Liu, S.; Andrade, G. A.; Hudson, D. A.; Scinto, S. L.; Dicker, K. T.; Li, Y.; Lazouski, N.; Rosenthal, J.; Thorpe, C.; Jia, X.; Fox, J. M. Rapid Bioorthogonal Chemistry Turn-on through Enzymatic or Long Wavelength Photocatalytic Activation of Tetrazine Ligation. *J. Am. Chem. Soc.* **2016**, *138*, 5978−5983.

(25) Liu, S.; Moore, A. C.; Zerdoum, A. B.; Zhang, H.; Scinto, S. L.; Zhang, H.; Gong, L.; Burris, D. L.; Rajasekaran, A. K.; Fox, J. M.; Jia, X. Cellular Interactions with Hydrogel Microfibers Synthesized Via Interfacial Tetrazine Ligation. *Biomaterials* **2018**, *180*, 24−35.

(26) Zhang, H.; Dicker, K. T.; Xu, X.; Jia, X.; Fox, J. M. Interfacial Bioorthogonal Cross-Linking. *ACS Macro Lett.* **2014**, *3*, 727−731.

(27) Dicker, K. T.; Song, J.; Moore, A. C.; Zhang, H.; Li, Y.; Burris, D. L.; Jia, X.; Fox, J. M. Core−Shell Patterning of Synthetic Hydrogels Via Interfacial Bioorthogonal Chemistry for Spatial Control of Stem Cell Behavior. *Chem. Sci.* **2018**, *9*, 5394−5404.

(28) Hao, Y.; Song, J.; Ravikrishnan, A.; Dicker, K. T.; Fowler, E. W.; Zerdoum, A. B.; Li, Y.; Zhang, H.; Rajasekaran, A. K.; Fox, J. M.; Jia, X. Rapid Bioorthogonal Chemistry Enables in Situ Modulation of the Stem Cell Behavior in 3D without External Triggers. *ACS Appl. Mater. Interfaces* **2018**, *10*, 26016−26027.

(29) Dicker, K. T.; Moore, A. C.; Garabedian, N. T.; Zhang, H.; Scinto, S. L.; Akins, R. E.; Burris, D. L.; Fox, J. M.; Jia, X. Spatial Patterning of Molecular Cues and Vascular Cells in Fully Integrated Hydrogel Channels Via Interfacial Bioorthogonal Cross-Linking. *ACS Appl. Mater. Interfaces* **2019**, *11*, 16402−16411.

(30) Doillon, C. J.; Dunn, M. G.; Bender, E.; Silver, F. H. Collagen Fiber Formation in Repair Tissue: Development of Strength and Toughness. *Collagen Relat. Res.* **1985**, *5*, 481−492.

(31) Tong, Z.; Duncan, R. L.; Jia, X. Modulating the Behaviors of Mesenchymal Stem Cells Via the Combination of High-Frequency Vibratory Stimulations and Fibrous Scaffolds. *Tissue Eng., Part A* **2013**, *19*, 1862−1878.

(32) Wagner, J. M. *X-Ray Photoelectron Spectroscopy: Chemical Engineering Methods and Technology*; Nova Science Publishers, Inc.: Hauppauge, NY, 2013.

(33) Yang, X.; Cui, C.; Tong, Z.; Sabanayagam, C. R.; Jia, X. Poly(Epsilon-Caprolactone)-Based Copolymers Bearing Pendant Cyclic Ketals and Reactive Acrylates for the Fabrication of Photocrosslinked Elastomers. *Acta Biomater.* **2013**, *9*, 8232−8244.

(34) Tong, Z.; Sant, S.; Khademhosseini, A.; Jia, X. Controlling the Fibroblastic Differentiation of Mesenchymal Stem Cells Via the Combination of Fibrous Scaffolds and Connective Tissue Growth Factor. *Tissue Eng., Part A* **2011**, *17*, 2773−2785.

(35) Swindle-Reilly, K. E.; Paranjape, C. S.; Miller, C. A. Electrospun Poly(Caprolactone)-Elastin Scaffolds for Peripheral Nerve Regeneration. *Prog. Biomater.* **2014**, *3*, 20.

(36) Taylor, M. T.; Blackman, M. L.; Dmitrenko, O.; Fox, J. M. Design and Synthesis of Highly Reactive Dienophiles for the Tetrazine-Trans-Cyclooctene Ligation. *J. Am. Chem. Soc.* **2011**, *133*, 9646−9649.

(37) Vaughan, M. B.; Howard, E. W.; Tomasek, J. J. Transforming Growth Factor-Beta1 Promotes the Morphological and Functional Differentiation of the Myofibroblast. *Exp. Cell Res.* **2000**, *257*, 180−189.

(38) Liao, J. K.; Seto, M.; Noma, K. Rho Kinase (Rock) Inhibitors. J. Cardiovasc. *J. Cardiovasc. Pharmacol.* **2007**, *50*, 17−24.

(39) Huang, X.; Yang, N.; Fiore, V. F.; Barker, T. H.; Sun, Y.; Morris, S. W.; Ding, Q.; Thannickal, V. J.; Zhou, Y. Matrix Stiffness−Induced Myofibroblast Differentiation Is Mediated by Intrinsic Mechanotransduction. *Am. J. Respir. Cell Mol. Biol.* **2012**, *47*, 340−348.

(40) Li, C. X.; Talele, N. P.; Boo, S.; Koehler, A.; Knee-Walden, E.; Balestrini, J. L.; Speight, P.; Kapus, A.; Hinz, B. Microrna-21 Preserves the Fibrotic Mechanical Memory of Mesenchymal Stem Cells. *Nat. Mater.* **2017**, *16*, 379−389.

(41) Branco, A.; Bartley, S. M.; King, S. N.; Jette, M. E.; Thibeault, S. L. Vocal Fold Myofibroblast Profile of Scarring. *Laryngoscope* **2016**, *126*, E110−E117.

(42) Akhmetshina, A.; Dees, C.; Pileckyte, M.; Szucs, G.; Spriewald, B. M.; Zwerina, J.; Distler, O.; Schett, G.; Distler, J. H. Rho-Associated Kinases Are Crucial for Myofibroblast Differentiation and Production of Extracellular Matrix in Scleroderma Fibroblasts. *Arthritis Rheum.* **2008**, *58*, 2553−2564.

(43) Torr, E. E.; Ngam, C. R.; Bernau, K.; Tomasini-Johansson, B.; Acton, B.; Sandbo, N. Myofibroblasts Exhibit Enhanced Fibronectin Assembly That Is Intrinsic to Their Contractile Phenotype. *J. Biol. Chem.* **2015**, *290*, 6951−6961.

(44) Goffin, J. M.; Pittet, P.; Csucs, G.; Lussi, J. W.; Meister, J. J.; Hinz, B. Focal Adhesion Size Controls Tension-Dependent Recruitment of Alpha-Smooth Muscle Actin to Stress Fibers. *J. Cell Biol.* **2006**, *172*, 259−268.

(45) Omachi, T.; Ichikawa, T.; Kimura, Y.; Ueda, K.; Kioka, N. Vinculin Association with Actin Cytoskeleton Is Necessary for Stiffness-Dependent Regulation of Vinculin Behavior. *PLoS One* **2017**, *12*, No. e0175324.

https://dx.doi.org/10.1021/acsmacrolett.0c00515
ACS Macro Lett. XXXX, XXX, XXX−XXX